Materials Horizons

REVIEW

View Article Online
View Journal | View Issue

Cite this: *Mater. Horiz.*, 2020, 7, 746

Recent developments in polydopamine fluorescent nanomaterials

Peng Yang,[a] Shu Zhang,[a] Xiaofeng Chen,[a] Xianhu Liu,[b] Zhao Wang*[c] and Yiwen Li*[a]

Polydopamine (PDA) fluorescent materials have recently gained much attention due to their unique physicochemical and biological properties. Since the first report on fluorescent PDA nanoparticles, many efforts have been made to develop new fabrication strategies to achieve their desirable luminescence properties. This feature article summarizes the recent advances and current highlights in fluorescent PDA materials including fabrication methods, nanomaterial morphologies, luminescence mechanisms and applications for imaging and sensing in the last few years. We believe that this review will provide new insights into the mechanistic aspect of PDA fluorescence for guiding preparation approaches and new applications.

Received 1st August 2019,
Accepted 11th November 2019

DOI: 10.1039/c9mh01197h

rsc.li/materials-horizons

1. Introduction

Polydopamine (PDA) is one of the most well-developed melanin-mimicking materials possessing attractive properties such as antioxidant activity, high photothermal conversion efficiency and strong metal ion chelation.[1–4] In 2007, Messersmith *et al.* reported a simple and facile method for a universal surface coating using PDA chemistry.[5] In their work, dopamine (DA) was employed as an adhesive building block that could self-polymerize in solution to form a PDA film on substrates. Based on this pioneering work, PDA-based materials have been intensively investigated as 3D nanoparticles (NPs), 2D surface coating/interface materials, 1D polymers and 0D dots in the past 10 years.[6–12] More importantly, bio-inspired PDA materials have been applied as multifunctional platforms for various biomedical applications, such as medical imaging, cancer therapy and tissue engineering.[13–22]

The high affinity of PDA for various metal ions and metal oxides is an attractive feature in medical imaging, including magnetic resonance imaging (MRI), photoacoustic imaging (PAI), positron emission tomography (PET) imaging, *etc.*[23–27] Fluorescence, another source of widely used medical imaging techniques, has been less integrated in the PDA-based imaging platforms due to its extremely low radiative quantum yields and efficient UV and visible energy dissipation characteristics.[28] To solve this, fluorescent molecules (dyes) have been incorporated into PDA for use in fluorescence imaging and sensing.[29,30] However, PDA was found to be a fluorescence quencher by Förster resonance energy transfer (FRET) and/or photoinduced electron transfer (PET) mechanisms, which may affect the fluorescence intensity of the attached dye molecules.[31–35] This motivated further engineering of the inherent stacking microstructure of PDA for turning its non-fluorescence nature into a fluorescence feature. Wei *et al.* first reported fluorescent PDA with excellent biocompatibility. The fluorescent PDA could be obtained by the oxidation of PDA NPs using H_2O_2,[36] which destroyed the original functional groups and surface structure of PDA. Although the aggregation-induced emission (AIE)-active polymeric nanoparticles are expected to monitor a dynamic process involving assembly behaviors, biological imaging, and theranostics,[37,38] fluorescent PDA can exhibit a novel mechanism as well as many advantages including facile synthesis, good biocompatibility, and rich surface functionalities. To date, some other kinds of strategies have also been developed to fabricate fluorescent PDA materials with outstanding properties and these strategies include degradation, conjugation, and carbonization. These fabrication strategies provide PDA nanomaterials with strong fluorescence intensity, which can be applied for various analysis and detection applications.

In this feature article, we explore the recent progress and future perspective of PDA-based fluorescent materials for imaging and sensing. The fabrication strategies for fluorescent PDA materials are summarized in the first section. We carefully reviewed the fluorescence generation mechanisms of the PDA materials. However, PDA materials with fluorescence originating from chemical conjugation or physical absorption of small fluorescent molecules are not discussed in this review. In the second section, we outline the recent advances in the structural

[a] College of Polymer Science and Engineering, State Key Laboratory of Polymer Materials Engineering, Sichuan University, Chengdu 610065, China. E-mail: ywli@scu.edu.cn
[b] National Engineering Research Center for Advanced Polymer Processing Technology, Zhengzhou University, Zhengzhou 450002, China
[c] Pritzker School of Molecular Engineering, University of Chicago, Chicago, Illinois 60637, USA. E-mail: zwang12@uchicago.edu

engineering of fluorescent PDA. The last section focuses on the applications of fluorescent PDA materials, including the intrinsic fluorescence of PDA and also fluorescent dye in PDA, for imaging and sensing. We believe this review provides the first summary of this specific new type of fluorescent material and a complement to polydopamine research. It will also promote the development and applications of fluorescent PDA materials and be of general interest to researchers in chemistry, analysis, material, and biology.

2. Fabrication strategy

The classic PDA synthesis involves the self-oxidation of DA into quinone under an alkaline environment and results in a chemical disorder model with non-covalent self-assembly and covalent polymerization.[39] The planar aromatic rings of PDA could quench fluorescence by the aggregation-caused quenching (ACQ) effect.[40,41] However, it was found that natural melanin, sharing structural similarity with PDA, could still emit luminescence radiatively under UV irradiation. Natural melanin possessed extremely low (<0.1%) radiative relaxation quantum yields and most of the absorbed energy dissipated in a nonradiative form.[28,42,43] Similarly, PDA showed weak and wavelength-dependent fluorescence under UV irradiation, which might account for the chemical disorder model.[44,45] It was observed that the complex and heterogenous chemical and physical microstructures within PDA intensively influence its fluorescence emission. Its high degree of polymerization caused strong entanglement of the molecule chains, forming intramolecular or intermolecular stacking of backbones that was unfavorable for fluorescence emission.[46,47] Previous literature has reported that the oligomers of DA were the main source of strong fluorescence due to the lower degree of π–π interaction.[48,49] Thus, the key to generating fluorescence from PDA is to suppress the DA polymerization or reduce the π–π stacking interaction between the structural units in PDA. Based on this, four fabrication strategies have been proposed by different groups during the most recent years: oxidation, degradation, conjugation, and carbonization. In particular, the chemical oxidation and degradation methods aim to regulate the π–π stacking interaction inside PDA *via* chemical oxidation or degradation treatment. The treated PDA materials with weaker π–π stacking interaction showed enhanced luminescence properties under UV excitation (Scheme 1). The conjugation strategy focused on the inhibition of DA polymerization *via* the introduction of additives or tuning the polymerization conditions so that the intermolecular or intramolecular coupling was hindered. Lastly, carbonization of PDA created distinct sp^2 hybridized carbon atoms inside the NPs to offer fluorescence. Table 1 summarizes the recent advances in typical fabrication strategies for fluorescent PDA materials.

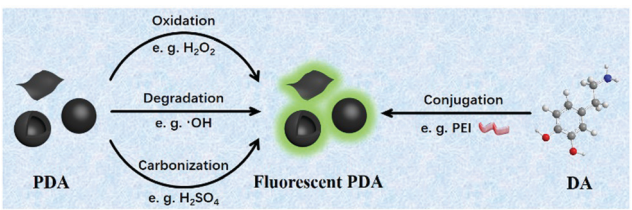

Scheme 1 Four typical fabrication strategies for fluorescent PDA nanomaterials.

2.1 Chemical oxidation

The inherent disorder from intermolecular or intramolecular conjugations within PDA resulted in efficient fluorescence quenching. The PDA oligomer is intrinsically fluorescent,[50,80] since a low degree of polymerization can effectively prevent π–π stacking. Chemical oxidation, by introducing polar groups into the system, can promote structural rearrangement to suppress the π–π stacking. Therefore, this method was applied to fabricate fluorescent PDA *via* adding oxidants either during (so-called pre-polymerization modification) or after (so-called post-polymerization modification) the polymerization process.[56,58] H_2O_2, as a green oxidant, was first introduced for preparing fluorescent PDA in 2012.[36] The obtained fluorescent PDA NPs were prepared in 5 hours without metal catalysts and avoiding complicated chemical synthesis processes. The resulting NPs showed good biocompatibility and luminescence and thus were used for efficient cell bioimaging.[36] However, the penetration depth of UV light was a concern which has promoted the development of fluorescent materials excited at higher wavelengths for better penetration depth. For example, Ma *et al.* very recently reported a post-polymerization modification method to produce fluorescent PDA *via* H_2O_2 oxidation (Fig. 1a). Importantly, the as-synthesized fluorescent PDA NPs showed not only one-photon but also two-photon fluorescence properties.[55] As shown in Fig. 1b, the fluorescent PDA NPs emitted bright blue to red light under excitation wavelengths from 350 to 500 nm. The PDA NPs also exhibited high two-photon fluorescence properties, showing broad emission peaks at around 530 nm under different excitation wavelengths from 760 to 900 nm (Fig. 1c). The two-photon quantum yield was about 6.4%. Compared with conventional fluorescein, the two-photon fluorescence occurred under near infrared (NIR) light, which allows imaging of living tissue up to about one millimeter in depth.

Besides H_2O_2, several other kinds of oxidants, including CoOOH nanosheets and MnO_2, were also used to produce fluorescent PDA *via* pre-polymerization modification.[59–62,64,65] In these examples, the oxidation and polymerization of the quinone units occurred simultaneously, resulting in a high proportion of carbonyl and carboxyl groups in the NPs. Although the carbonyl and carboxyl groups were electron-accepting moieties, which promote non-radiative processes and quench fluorescence,[81] they prevented the formation of π–π interaction during the polymerization, so that the fluorescence of PDA was improved due to the mitigation of fluorescence quenching.[47] Generally, the fluorescence intensity increased gradually with the increase of oxidant concentration. However, too much oxidant might cause fluorescence quenching due to the formation of large-scale aggregations.[60,82] Apart from the oxidant concentration, reaction time and pH also had significant influence. For example, polymerization of DA was

Table 1 A brief summary of typical fabrication strategies for fluorescent PDA nanomaterials and their related applications

Method	Treatment	λ_{Ex}/nm	λ_{Em}/nm	QY/%	Applications	Ref.
Chemical oxidation	O_2	370	510	—	DA detection	50
		360–420	415	—	Biosensing	51
		310–530	450–610	9.1	Glu and Al^{3+} detection	52
	H_2O_2	360–500	380–560	—	Bioimaging	36
		488	510–550	—	Electronic imaging	53
		400	480	—	Bioimaging	54
		760–900	530	6.4	Bioimaging	55
	H_2O_2/Fe_3O_4	480	530	1.0	Zn^{2+} detection	56
	H_2O_2/MnO_2	393	500	—	Alpha-fetoprotein detection	57
	H_2O_2/ficin	400	476	—	DA detection	58
	MnO_2	400	485	—	GSH detection	59
	CoOOH	400	500	—	Ascorbic acid detection	60
	$NaIO_4$	380	455	5.1	Fe^{3+} detection	61
	EDC	350–440	465	35.8	Nucleus fluorescence labeling	62
	Trypsin	317	490	5.8	Fe^{3+} detection	63
	Hydrothermal	310–360	500	93	Cr^{6+} detection	64
	$KMnO_4$	390	500	1.09	ALP activity detection	65
	Microplasma electrochemistry	360	440	0.58	Uranium detection	66
	Plasma	340	430	0.8	Bioimaging	67
	UV	405, 488	460–650	—	Tocopherol sensing	68
Degradation	EDA	340–480	510	—	Bioimaging	69
	Hydroxyl radicals	300–500	447–556	1.2	Fe^{3+} detection	49
Conjugation	PEI	380	526	—	Bioimaging	70
		350	508	—	DA detection	71
		400	520	—	—	72
	GSH	320–450	480–540	5.6	Cu^{2+} and Fe^{3+} detection	73
		360	450	3.3	Establishment of logic gate	74
		380	450	—	H_2O_2 and glucose detection	75
	Glycine	360–440	485	16.2	Bioimaging	48
	Starch	365	500	—	Bioimaging	76
Carbonization	H_2SO_4	300–460	490–510	2.90[a] 8.80[b]	Photothermal therapy	77
		365	465	—	Bioimaging	78
	H_2SO_4, PEI	360	pH dependent	1.33	Bacterial sensing	79

[a] The quantum yield of the fluorescent PDA under 405 nm. [b] The quantum yield of the fluorescent PDA under 488 nm. QY: quantum yield, DA: dopamine, Glu: glutamate, GSH: glutathione, EDC: *N*-(3-(dimethylamino)propyl)-*N*-ethylcarbodiimide, ALP: alkaline phosphatase, EDA: ethylenediamine, PEI: polyethyleneimine.

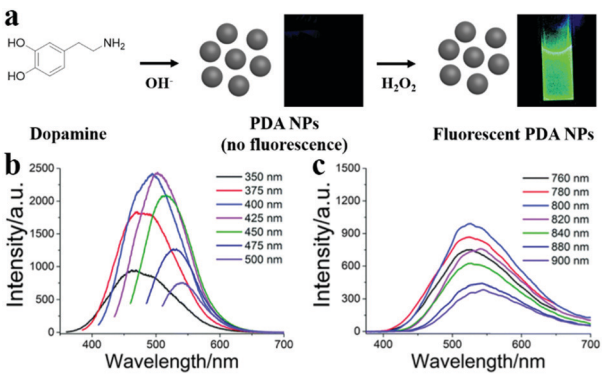

Fig. 1 (a) Schematic illustration of the fluorescent PDA NP synthesis. (b) One-photon emission spectra of fluorescent PDA under different excitation wavelengths. (c) Two-photon emission spectra of fluorescent PDA under different excitation wavelengths.[55] Reproduced from ref. 55 with permission from the Royal Society of Chemistry.

accelerated at basic pH while the fluorescence of PDA was enhanced at neutral or acidic pH due to inhibition of the uncontrolled autoxidation process.[61] However, there was still an excess of electron-accepting carbonyl and carboxyl moieties on the surface of PDA after oxidation that could quench the fluorescence and induce a non-radiative recombination process, leading to low quantum yield. To solve this, Fu's group employed $NaBH_4$ as the reductant to convert carbonyl and carboxyl moieties into hydroxyl groups (Fig. 2)[61] that could suppress non-radiative processes and further enhance the integrity of the π-conjugated system as the electron donor.[83] Moreover, based on the electron-donating feature, hydroxyl groups also could enhance the luminescence of PDA. After $NaBH_4$ treatment (8%, w/v) for 24 h, the fluorescence intensity was significantly enhanced and the quantum yield was determined to be 5.1%. These results revealed the relationship between the manipulation of the surface chemistry of PDA and its potential photoluminescence mechanism. More specifically, it is important for fluorescence enhancement to decrease the amount of electron-withdrawing groups, such as carbonyl and carbonyl groups, which have quenching effects and attract non-radiative recombination processes. In contrast, electron-donating groups (*e.g.*, hydroxyl groups) could further integrate the electron structure and enhance the luminescence.

These oxidants can effectively accelerate the oxidation process and shorten the reaction time. This kind of metal material-based oxidant also can selectively cooperate with other molecules to develop new sensing devices with excellent

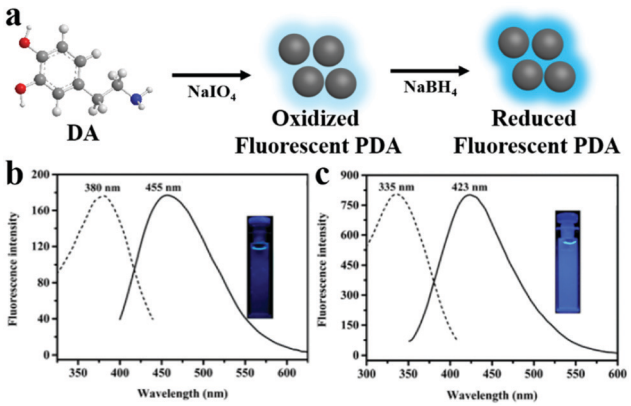

Fig. 2 (a) Schematic illustration of the preparation of fluorescent PDA. Optimal excitation and emission spectra of oxidized fluorescent PDA (b) and reduced fluorescent PDA (c). The dashed lines and solid lines are excitation curves and emission curves, respectively.[61] Reproduced from ref. 61 with permission from the Royal Society of Chemistry.

performance based on PDA. It is worth mentioning that the toxicity of harsh oxidants is a concern that has not yet been well addressed. Besides chemical oxidants as mentioned above, micro-plasma electrochemistry and UV irradiation treatments were also successfully employed to synthesize fluorescent PDA. Treating the DA solution with a micro-plasma anode not only generated oxidative species to trigger the formation of PDA NPs at the plasma–liquid interface, but also provided an acidic environment to terminate the oxidation reaction to avoid aggregates.[66] The fluorescence intensity increased with increase of the treatment time, reaction current and initial DA concentration, which resulted in generation of more oxygen radicals produced by plasma.[66] Furthermore, fluorescent PDA materials were also prepared *via* UV irradiation. Quignard *et al.* demonstrated the synthesis of fluorescent PDA-coated core–shell droplets *via* UVA illumination.[68] The results showed that UVA irradiation induced the photooxidation of uncyclized catecholamine units into cyclized fluorescent units (Fig. 3), since 5,6-dihydroxyindole (DHI) and the dimers in their reduced state exhibited significant emission properties.[84] The fluorescence can be stabilized by borate and even enhanced by Tris, which prevented the over-oxidation and cyclization.[85] It was also found that vegetable oils and inert mineral oils could effectively induce fluorescence emission because of the good solubility of fluorescent DHI components in oil.

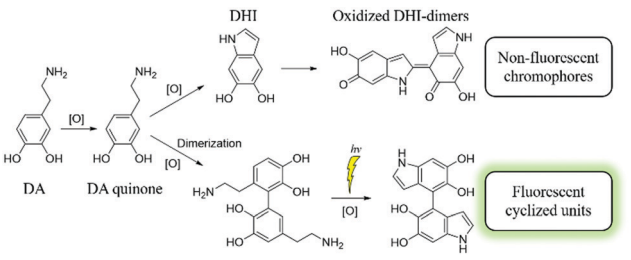

Fig. 3 Schematic illustration of DA polymerization and pathways leading to either nonfluorescent or fluorescent moieties.[68] Copyright © 2014 Wiley-VCH Verlag GmbH & Co. KGaA, Weinheim.

2.2 Degradation

Although the structure of PDA is still under debate, it is a consensus that π–π stacking interaction between the oligomeric units could result in the quenching of fluorescence. Degradation methods that destroy the π–π stacking interaction could be employed to prepare fluorescent PDA. Furthermore, the size of PDA usually becomes smaller after degradation. The fluorescence originated from small fluorescent parts formed during the degradation, rather than from the existing PDA NPs.[69] Hydroxyl radicals are known to degrade PDA *via* radical coupling to form hydroxyldopamines, such as 2-hydroxyldopamine, 5-hydroxyldopamine, and 6-hydroxyldopamine. Lin *et al.* used high concentration H_2O_2 as a hydroxyl radical source to degrade PDA under a strong alkaline condition (Fig. 4).[49] The additional hydroxyl groups would reduce the π–π stacking interactions between the microscopic units within PDA, resulting in the formation of strongly fluorescent PDA particles. The maximal emission shifted from 477 to 556 nm with the increase of excitation wavelength from 300 to 500 nm and the quantum yield was calculated to be 1.2%.[49] These results demonstrated that the maximal peaks of fluorescence emission strongly depend on the excitation wavelengths, since the NPs contained complex structural units, such as 5,6-dihydroxyindole and trihydroxylindole units, that had different energy levels.[49] Ethylenediamine (EDA) also can induce degradation of PDA and the products exhibited excellent water dispersity.[69] The fluorescence intensity reached a maximum at 510 nm with the excitation wavelength of 400 nm. Compared with chemical oxidation strategies, the degradation method caused a size reduction in raw materials, leading to a lower degree of oligomerization and self-assembly, as proved by the peak intensity decrease in the FT-IR spectrum.[49] Moreover, the fluorescence properties of the PDA were stable under high-ionic-strength conditions, as well as in a wide pH range. However, the degradation mechanism of PDA has not been fully understood.

2.3 Conjugation

DA monomers can self-polymerize to form PDA under alkaline environment without additional catalysis. To eliminate the stacking interaction of PDA, amine- or thiol-containing organic species were used in the polymerization process of DA *via*

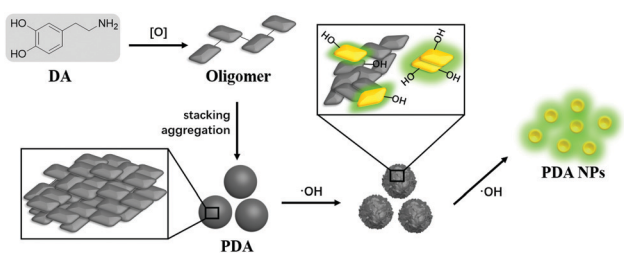

Fig. 4 Schematic illustration of the synthetic procedure for fluorescent PDA NPs.[49]

Schiff base or Michael addition reaction to prevent dopamine cyclization.[86,87] These extra organic species were found to decrease the polymerization degree of DA and eliminate the stacking interaction to generate fluorescence. In 2015, Liu *et al.* reported the synthesis of fluorescent PDA NPs *via* co-polymerization of DA and polyethyleneimine (PEI) (Fig. 5a).[70] PEI not only provided the alkaline environment to promote dopamine polymerization but also reacted with dopamine, mainly *via* Michael addition reaction and partly *via* Schiff-based reaction (Fig. 5b), to prevent cyclization.[72] It was found that the size of the resulting PDA–PEI NPs became smaller and their fluorescence intensity became stronger as the concentration of PEI increased.[72] It might be concluded that PEI reduced the aggregation of PDA, thereby weakening the intermolecular coupling effect, and resulted in fluorescence enhancement compared to that of PDA. The PDA–PEI NPs exhibited strong green fluorescence, with excitation and emission wavelengths of 380 nm and 526 nm, respectively (Fig. 5c).[70] Interestingly, the emission wavelength of the products was found to be independent of the excitation wavelength (Fig. 5c). The authors also investigated the effect of other additives, including polyvinyl pyrrolidone (PVP) and diethylenetriamine (DETA).[72] PVP can only form hydrogen-bonds with PDA, which induced the formation of fluorescent PDA–PVP with an emission peak at 501 nm. However, the fluorescence intensity was much weaker than PDA–PEI. Therefore, it could be proved that the conjugation and the hydrogen-bonding interactions induced by PEI are not the sole reasons for the enhancement of fluorescence of PDA–PEI. Moreover, lower intensity of fluorescence was observed when replacing PEI with DETA at the same concentration. Thus, the enhancement of fluorescence of PDA–PEI was attributed to the Michael addition of PEI on the DHI unit, forcing the polymer to twist out of plane so that intra- and intermolecular coupling were reduced.

Glutathione (GSH), an endogenous molecule, was also employed to produce fluorescent PDA *via* a straightforward one-pot method under mild conditions.[73] GSH was found to react with PDA using the Michael addition reaction and to reduce the self-quenching effects. To shorten the reaction time, H_2O_2 was added to accelerate the formation of fluorescent PDA NPs (Fig. 6a). Combined with H_2O_2, the as-synthesized PDA NPs possessed enhanced fluorescence (Fig. 6b), with excitation and emission peaks of 360 nm and 450 nm (Fig. 6c), respectively. The fluorescence intensity of the NPs gradually increased at first and reached its maximum when using 250 μL H_2O_2. However, excess H_2O_2 induces DA to form precipitates and decreases the fluorescence intensity of the NPs.[45] In general, PDA showed a broadband absorption caused by the interplay of orderly and disorderly PDA.[74,88] In contrast, the absorption spectrum became narrower in the present of GSH, indicating that GSH could reduce the disordered part of PDA. Furthermore, the existence of thiol groups, rather than carboxyl, amino or peptide groups, was the important factor for enhancing the fluorescence.[75] The results showed that GSH significantly enhanced the fluorescence intensity and emitted blue light under UV excitation while other thiol-free amino acids showed no enhancement (Fig. 6d). The authors hypothesized that the presence of thioether groups formed by GSH and PDA microstructures could prevent photoinduced intramolecular electron transfer, which might be the reason for the low fluorescence intensity. However, excess H_2O_2 can further oxidize thioether to sulfoxide or sulfone groups,[89] which might enhance the electron-withdrawing ability, resulting in a decrease in fluorescence intensity. Note that the main function of H_2O_2 was to provide an oxygen resource to promote the synthesis of fluorescent PDA.[75] Precise control of H_2O_2 concentration is necessary to prevent the oxidation of thioether groups.

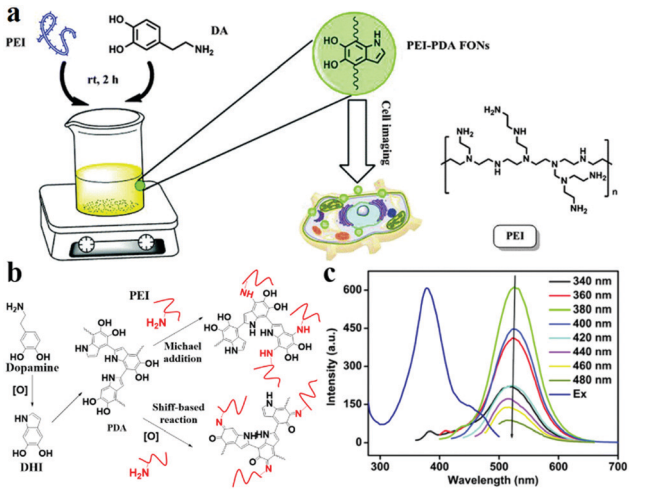

Fig. 5 (a) Schematic illustration of fluorescent PDA preparation through co-polymerization with DA and PEI.[70] (b) Schematic illustration of the two possible formation processes of the PDA–PEI copolymer.[72] (c) Fluorescence emission spectra of PDA–PEI (in water).[70] Reproduced from ref. 70 with permission from the Royal Society of Chemistry.

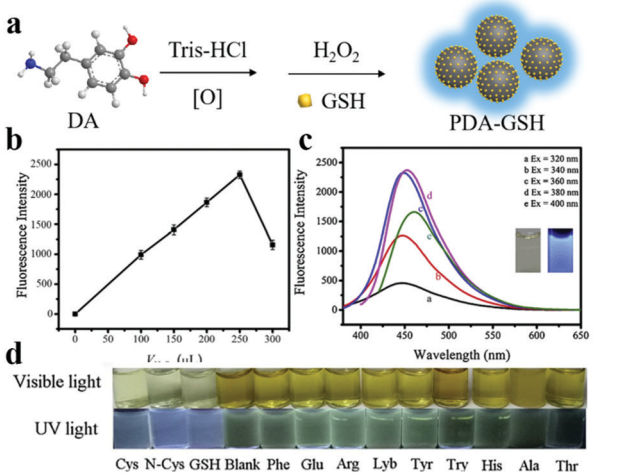

Fig. 6 (a) Schematic illustration of the preparation of fluorescent PDA NPs using GSH. (b) The effect of increasing H_2O_2 volume on the fluorescence intensity of DA and GSH system. (c) Fluorescence emission spectra of fluorescent PDA NPs under different excitations from 320 to 400 nm.[74] (d) Images of the appearance changes when various reactants were added to dopamine solutions with H_2O_2.[75] Reproduced from ref. 74 and 75 with permission from Elsevier.

Here, the conjugation strategy mainly aimed at tuning the inter- and intramolecular coupling structures and electron transfer structure of PDA and different conjugated molecules might induce various emissions. However, the debatable polymerization process of PDA caused uncertainty of the final products based on different conjugated molecules. Therefore, more precise molecular structure details and more effective characterization methods are needed to predict these changes.

2.4 Carbonization

Luminescent carbonized NPs from different natural and artificial sources, usually exhibiting excellent photostability, favorable biocompatibility and good water dispersity, have attracted much attention in recent years. Various mechanisms have been proposed to study the fluorescence origin of carbonized nanomaterials, including free zigzag sites, coexistence of defect state emission and intrinsic state emission, and electron transition.[90–92] Particularly, carbonization of organic NPs has been recognized as the standard method to prepare carbonized NPs.[93] PDA NPs, which are easily produced in large scale, have been utilized as the carbon source. Generally, the carbonization of nanomaterials is carried out by high temperature or strong acid (*e.g.* concentrated sulfuric acid). Interestingly, after carbonization *via* strong acid, PDA NPs are endowed with fluorescence. In contrast, carbonization with high temperature has not yet been reported to generate fluorescence. For instance, Kim *et al.* synthesized fluorescent PDA NPs through treatment of concentrated sulfuric acid, which can dehydrate PDA to induce luminescence (Fig. 7). The lattice separations (0.308 nm) were consistent with those of graphitic carbon structures. In the Raman spectrum, the fluorescent PDA NPs showed a clear G-band at 1590 cm^{-1} and a D-band at 1360 cm^{-1}, suggesting the presence of sp^2 and sp^3 hybridized carbons in these NPs. They also found that the surface passivation process using polyethylene glycol (PEG) improved the fluorescence of carbonized PDA NPs. The NPs showed excitation-dependent fluorescence emission (Fig. 7b and c). After the surface passivation with PEG, the surface ionic charge was shielded, which increased both fluorescence intensity and quantum yield (from 1.33% to 2.90% for blue and from 4.77% to 8.80% for green). These NPs showed no obvious cell toxicity after incubation with KB (oral carcinoma) or MDCK (Madin–Darby Canine Kidney) cells for 24 hours. The optoelectronic properties of such carbonized materials were strongly affected by the number and spatial distribution of conjugated bonds[94] and the sites of delocalized electrons, which can effectively alter the fluorescence properties of carbonized PDA.

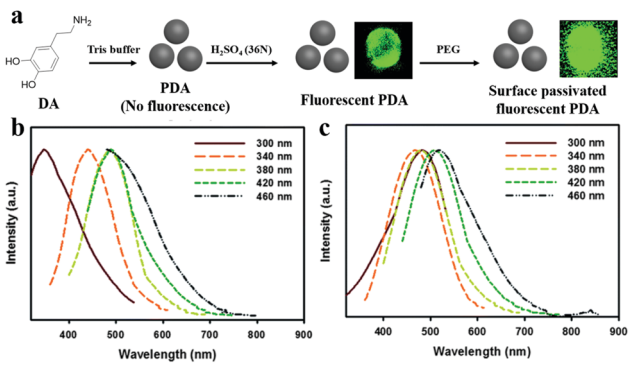

Fig. 7 (a) Schematic illustration of fluorescent PDA fabrication *via* carbonization and surface passivation strategy. The normalized fluorescence emission spectra of (b) PDA and (c) surface-passivated PDA at different excitation wavelengths (300–460 nm).[77] Reproduced from ref. 77 with permission from the Royal Society of Chemistry.

Surface passivation treatment was proposed to enhance the fluorescence of carbonized PDA NPs, since surface energy traps on such NPs become emissive upon stabilization as a result of the surface passivation. Moreover, a large surface-to-volume ratio is also favored for higher photoluminescence quantum yields. Sun *et al.* found that larger particles with the same surface passivation showed weaker fluorescence, suggesting the importance of quantum confinement of emissive energy traps to the particle surface.[91] However, controlling the ratio of sp^2 and sp^3 hybridized species during the carbonization process is still challenging. Therefore, we anticipate that methods will be developed to obtain well-defined hybridized structures of PDA after carbonization so that desirable fluorescence properties can be achieved.

3. Classification

The classification and nanoscale morphologies of fluorescent materials are essential to understand those complex multiphase systems for their biomedical, energy and aerospace applications.[95] So far, many efforts have been made for controlled fabrication of distinct types of fluorescent PDA materials accessing different morphologies, including oligomers, nano-sized particles and capsules, which may further achieve desirable properties.

3.1 Oligomers

PDA oligomers are a series of low molecular weight polymers consisting of DA and its derivatives, such as DHI and 5,6-dihydroxyindoles-2-carboxylic acid (DHICA). PDA oligomers can emit fluorescence when excited by UV light, while their aggregates do not show luminescence due to the ACQ effect. To reduce the degree of polymerization, additive molecules containing amino or thiol groups were added to hinder the cyclization reaction. Xiong *et al.* first employed glutaraldehyde and glycine to chemically conjugate to the amino groups of DA. The polymerization was initiated by ammonia solution and terminated with mercaptoethanol.[48] After polymerization, the purified oligomers exhibited bright glaucous fluorescence under 365 nm excitation, as well as higher quantum yield (16.2%) than in previous literature.[36] The fluorescence lifetime of the oligomers was measured to be ~2.35 ns and the fluorescence intensities of the oligomers had no obvious decrease under irradiation with 397 nm light for 1500 s, suggesting excellent photostability. Very recently, our group also synthesized fluorescent PDA oligomers *via* oxidative polymerization of DHI, DHICA and its derivatives 5,6-dihydroxyindoles-2-carboxylic acid methyl ester (DHICMe) and 5,6-dihydroxy

indole-2-carboxylic acid ethyl ester (DHICEt) under alkaline conditions.[96] According to the two-dimensional fluorescence contour maps, the emission wavelengths of all samples were excitation-dependent due to the existence of multiple oligomers. Interestingly, we found that the degree of polymerization was correlated to the fluorescence intensity, which could be used to analyze the polymerization to selectively prepare the fluorescent oligomers with desirable emission wavelengths and intensity. However, there were several oligomeric chemical structures formed in the polymerization and the main fluorescence source still needs to be explored.

3.2 Nano-sized particles

PDA dots and PDA NPs have been used in various studies; the diameter of PDA dots is usually less than 10 nm, while that of PDA NPs is larger. However, the subject of PDA dots is still under discussion. To simplify this, these dots and NPs are both classified as "nano-sized particles". PDA NPs are generally synthesized through spontaneous oxidation and self-polymerization of dopamine and the fluorescent PDA NPs have received much attentions for their potential applications in the fields of biomedicine, diagnosis and bioimaging.[69,97] The nano-sized PDA NPs were found to be suitable for labelling and imaging the cell as well as the organism. In general, the fabrication of fluorescent PDA NPs can be divided into "top-down" and "bottom-up" strategies, referring to the breaking down of large-size materials and pyrolysis or self-assembly of small organic molecules, respectively. Accordingly, PDA NPs can be obtained by strong chemical oxidation or degradation of EDTA or radicals.[49,64] During the polymerization process, the addition of oxidant, such as H_2O_2, usually lessens the stacking interactions between the structural units in PDA, endowing the PDA NPs, which had a size distribution ranging from a few to hundreds of nanometers, with luminescence.[36,53,56,58,74] For example, Zhao *et al.* reported the synthesis of fluorescent PDA NPs *via* a simple hydrothermal method under an acidic environment.[64] The obtained PDA NPs, with an average diameter of 3.02 nm, showed not only remarkable photoluminescent properties but also high stability. The quantum yield reached 93% under optimum excitation and the Stokes shift also suggested a weak self-absorption effect and low energy loss. However, the intense oxidation treatment and complicated synthesis might hinder the further applications due to safety and economic concerns. To avoid this, Ci *et al.* prepared fluorescent PDA NPs *via* three months of natural oxidation in air without additional oxidizing agent (Fig. 8a), where the solution was prepared and simply kept in the dark.[52] These PDA NPs, with a relatively narrow size distribution, exhibited characteristics of amorphous carbon and nanocrystalline graphite structures (Fig. 8b). The optical properties were explored by fluorescence spectra, showing the excitation-dependent-emission phenomenon (Fig. 8c), which might be explained by the various "surface states" formed by diverse functional groups and the size effect, known as the quantum confinement effect.[98] The quantum confinement effect is the most accepted mechanism model for carbon nanostructures to explain the change of fluorescence emission

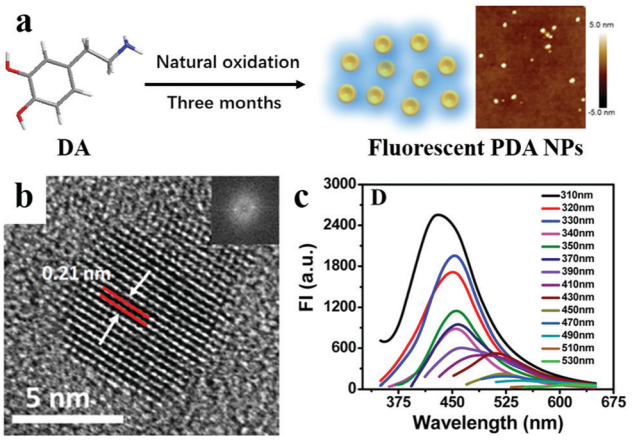

Fig. 8 (a) Schematic illustration of the preparation of fluorescent PDA NPs *via* natural oxidation. (b) High-resolution transmission electron microscopy (HRTEM) image of fluorescent PDA NPs. (c) Fluorescence spectra of fluorescent PDA NPs under different excitation wavelengths.[52] Reprinted with permission from ref. 52. Copyright 2018 American Chemical Society.

induced from different sizes, which could influence the energy gaps of these nanomaterials and broaden the emission wavelength.

Furthermore, PDA had fluorescent properties after several simple post-polymerization treatments, such as ethylene-diamine degradation or H_2SO_4 dehydration.[69,77] Dopamine could also be oxidized by NP-based oxidants or under plasma treatment to form several nanometer sized fluorescent PDA NPs.[60,66,67] For instance, Kong *et al.* reported that dopamine could be effectively oxidized and form its quinone derivates, which further polymerized to form fluorescent PDA NPs, after mixing with MnO_2 (Fig. 9a).[59] The resulting particles showed irregular shapes and a broad size distribution, suggesting relatively uncontrolled polymerization kinetics (Fig. 9b). Compared with MnO_2 and DA, a remarkable fluorescence

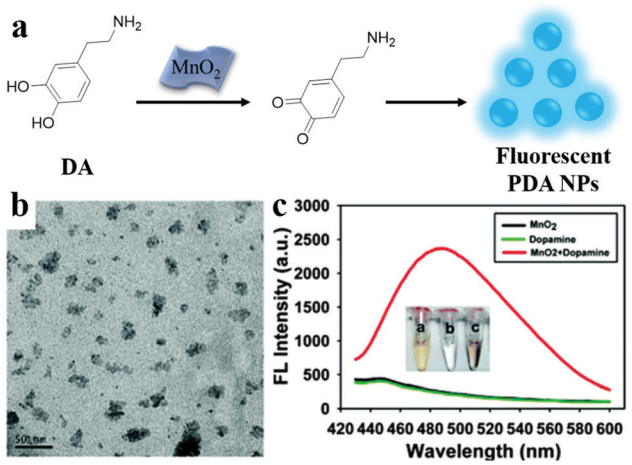

Fig. 9 (a) Schematic illustration of the synthesis of fluorescent PDA NPs. (b) TEM image of the fluorescent PDA NPs. (c) Fluorescence emission spectra of dopamine, MnO_2, and the mixture of dopamine and MnO_2.[59] Reproduced from ref. 59 with permission from the Royal Society of Chemistry.

signal was obtained after mixing DA with MnO_2 (Fig. 9c), suggesting the successful synthesis of fluorescent PDA NPs. Moreover, fluorescent PDA NPs can be prepared by controlling the degree of reaction *via* shortening reaction time, inhibiting the oxidization reaction, or blocking polymerization sites.[50,51,70,75] However, the high reactivity of dopamine and its derivatives makes it difficult to achieve a uniform morphology and unimodal size distribution within a short time to endow the NPs with stable scattering interference and diffusion coefficients.

3.3 Capsule

PDA capsules have attracted broad attention in many fields, such as delivery, storage and nanoreactors.[99–101] Typically, PDA capsules were synthesized by template-based methods, which can be divided into hard template, including SiO_2 and polystyrene microspheres,[102,103] and soft template, such as oil droplets, methods. The PDA coating on such templates' surfaces was easily achieved *via* a previously reported universal coating approach.[5] However, characterization of PDA capsules for *in vivo* applications, such as biodistribution, required the binding of high metal ion content as the tracer for inductively coupled plasma mass spectrometry (ICP-MS) analysis. To avoid the potential toxicity induced by foreign additives, PDA capsules were expected to integrate fluorescence so that the pharmacokinetics and biodistribution of these nanocarriers can be investigated. Caruso's group reported the template synthesis of PDA capsules using different hard templates, including SiO_2, polystyrene microspheres and $CaCO_3$, followed by H_2O_2 treatment to offer fluorescence (Fig. 10a).[54] The size of the capsule and the thickness of the shell can easily be controlled by tuning the size of template (capsule) and coating time, concentration and pH (shell). After the second coating with H_2O_2 treatment, the capsules exhibited bright green fluorescence with a fluorescein isothiocyanate (FITC) filter (excitation 555 ± 14 nm) (Fig. 10b). Importantly, the oxidation reaction time with H_2O_2 is one of the crucial parameters that influence the fluorescence property, where the fluorescence intensity gradually increased and reached a maximum at 15 h.

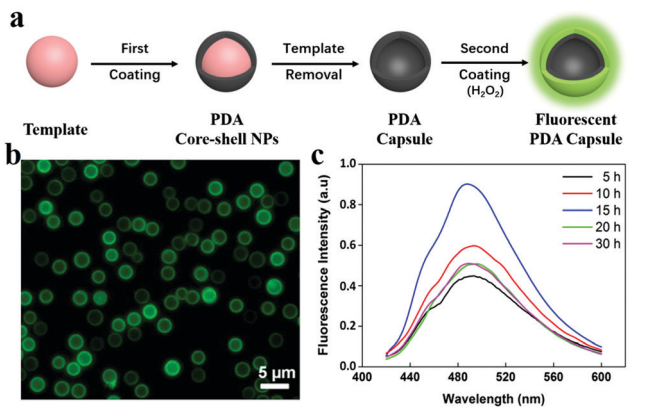

Fig. 10 (a) Schematic illustration for the synthesis of fluorescent PDA capsules. (b) Fluorescence microscopy image of the resulting fluorescent PDA capsules. (c) Normalized emission spectra of fluorescent PDA capsules using different H_2O_2 reaction times.[54] Reprinted with permission from ref. 54. Copyright 2014 American Chemical Society.

Excessive H_2O_2 treatment might degrade and destabilize the PDA structure, leading to a decrease of fluorescence intensity at longer reaction times (Fig. 10c). Furthermore, the fluorescent PDA capsules were easily observed by fluorescence microscope, which could be employed to quantitatively and qualitatively analyse the interaction between PDA materials and cell. Considering the variety of templates, it is expected that fluorescent PDA capsules with morphologies other than spherical can be achieved to meet requirements in specific conditions.

Hard templates have been successfully applied to construct PDA capsules. However, etching hard templates usually required harsh chemical reagents such as organic solvents and acid, which might hinder further applications of chemically sensitive materials. In contrast, a soft template can be easily removed under mild conditions. Quignard *et al.* employed oil-in-water emulsion droplets using different oils, including vegetable, mineral and silicone oils, to fabricate fluorescent PDA capsules.[68] Interestingly, fluorescence was observed with vegetable or mineral oil after UVA irradiation but not with silicone oil, which may be attributed to the poor penetration of PDA components in relatively more hydrophobic and apolar media. The photochemical processes of UVA could convert nonfluorescent moieties into emitting ones. The liquid organic interface and the deposition conditions would be in favor of fluorescence development, while avoiding extra chemical settlement and benefitting the development of relevant sensors for tocopherol in micromolar concentration. To date, most studies have mainly focused on the synthesis of the fluorescent PDA. The tunability of the fluorescence properties and further functionalization of fluorescent PDA have rarely been reported for multifunctional theranostics.

4. Applications

Fluorescent PDA nanomaterials have been widely used in the fields of imaging and sensing, due to their promising and tunable fluorescence properties, good water dispersity, biodegradability and biocompatibility. The tunability of fluorescence can endow PDA with the abilities to adapt in complex environments to meet different demands. Fluorescent PDA showed no obvious toxicity to cells or organisms, suggesting potential in bio-related applications. Compared with inorganic quantum dots and fluorescent dyes, fluorescent PDA can be easily engineered with other functional blocks to achieve multifunctional nanoplatforms, making fluorescent PDA an extremely promising fluorescent agent for imaging and sensing.

4.1 Bioimaging

Bioimaging refers to the imaging techniques aimed at noninvasively visualizing biological processes in real time, which have been used to analyze the morphology and characteristics of specific areas in the cell, tissue or organism. The imaging techniques used in bioimaging include fluorescence imaging, positron emission tomography, and optical tomography.[104,105] Fluorescence-based bioimaging is defined as the acquisition

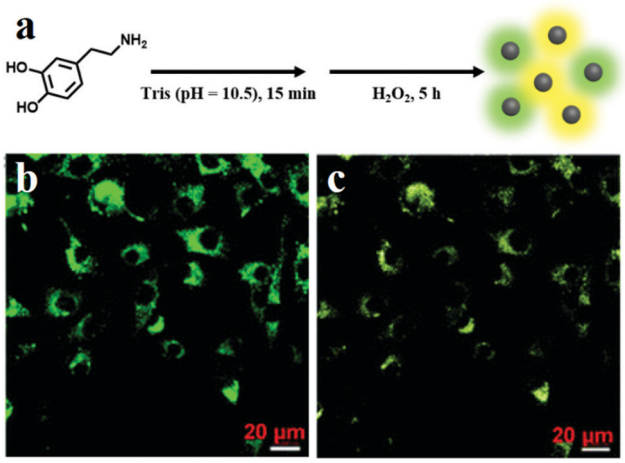

Fig. 11 (a) Schematic illustration of the synthesis of fluorescent PDA by H_2O_2 oxidation. Confocal laser scanning microscopy images of cells imaged under bright field 405 nm (b) and 458 nm (c) excitations.[36] Reproduced from ref. 36 with permission from the Royal Society of Chemistry.

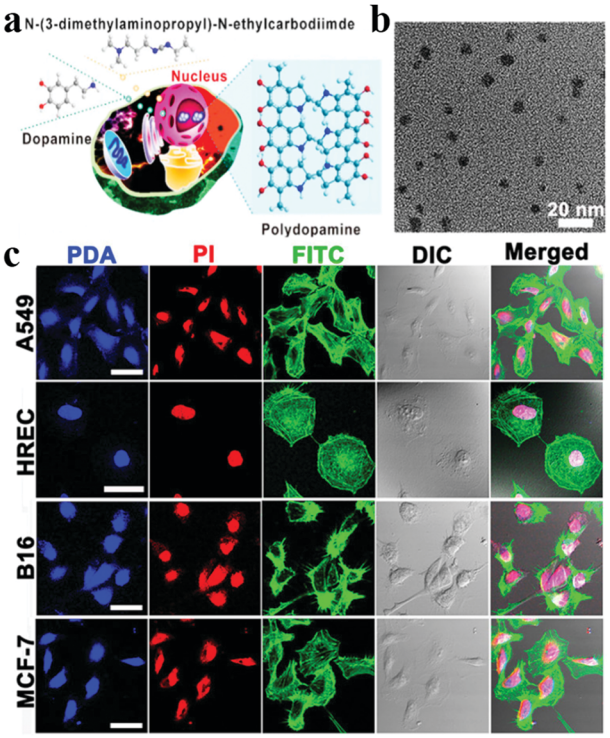

Fig. 12 (a) Schematic illustration of fluorescent PDA preparation for labelling live-cell nuclei. (b) TEM image of fluorescent PDA. (c) Colocalization images of A549 cells, HREC cells, B16 cells, and MCF-7 cells.[62] Reprinted with permission from ref. 62. Copyright 2017 American Chemical Society.

of images of biological matter using fluorescent probes, fluorescent labels or related fluorescent nanomaterials with high sensitivity, high selectivity and versatility.[106] Recently, PDA-based fluorescent nanomaterials have provided new possibilities for bioimaging. Zhang *et al.* first used fluorescent PDA, obtained *via* the H_2O_2 oxidation method, for cell imaging (Fig. 11a).[36] The emission peak of the fluorescent PDA moved to a higher wavelength when excitation increased from 360 to 500 nm and fluorescence intensity reached the maximum under 440 nm excitation. The cell incubated with PDA exhibited green and green-yellow fluorescence when excited at 405 and 458 nm, respectively, indicating the internalization and accumulation of fluorescent PDA in NIH-3T3 cells (Fig. 11b and c). This one-pot oxidation showed no obvious cytotoxicity with concentrations up to 160 μg mL^{-1}, suggesting promising safe utilization in bioimaging.

So far, a series of PDA-based fluorescence nanomaterials with excellent luminescence performance have been applied for bioimaging.[107–109] Ding *et al.* showed the first example of labelling live-cell nuclei *in situ* using fluorescent PDA NPs (Fig. 12).[62] DA and *N*-(3-(dimethylamino)propyl)-*N*-ethylcarbodiimide (EDC) were incubated with cells (A549, HREC, B16, and MCF-7) under physiological conditions for 3 h. EDC induced the polymerization of DA to prepare fluorescent PDA NPs. The fluorescent PDA NPs, with high quantum yield (35.8%), exhibited strong binding abilities with DNA and ribosome RNA (rRNA). The results showed that fluorescent PDA emitted its strongest light intensity at ~465 nm under the excitation wavelength of 420 nm. Moreover, less than 20% of fluorescence intensity was lost after 3 h of continuous UV irradiation, indicating relatively good photostability. Live-cell labelling experiments showed that the fluorescence of PDA was located at the nucleus, showing bright blue color without obvious background. This nucleus labelling result was further confirmed by propidium iodide (PI), a red-fluorescent nuclear stain, showing the overlapped locations at the nuclei with a blue (PDA) signal. FTIC was further used as a control to label the cellular microfilaments surrounding the nuclei. Compared with conventional fluorescence labelling approaches, this fluorogenic probe based on PDA showed excellent nucleus-targeting ability, good photostability, and great spectroscopic properties, offering a new clue to analyse subcellular structures at the single cell level and/or complex biological samples.

Fluorescent PDA NPs obtained *via* conjugation or degradation also possessed outstanding fluorescence stability and have been applied for bioimaging. The PDA–PEI reported by Liu *et al.* was effectively taken in by cells even at low concentration (10 μg mL^{-1}) and exhibited bright green fluorescence.[70] Mazrad *et al.* also found that the fluorescence decay time and fluorescence quantum yield were dependent on the ratio of PDA and PEI.[79] After incubation with bacteria, the fluorescence of the NPs was quenched significantly, resulting from ionic interactions between the cationic NPs and anionic bacteria.[79] Moreover, it was reported by Gu *et al.* that the fluorescent PDA NPs could selectively label neuromast hair cells in the supraorbital, otic and occipital/posterior lateral lines of zebrafish without any modification of targeting molecules *via* endocytosis or passing through large non-selective cationic channels (Fig. 13). Therefore, it has been used to quantify the number of functional hair cells per neuromast in live animals as development proceeds.[69] It was observed that the fluorescence intensity of the fluorescent PDA NPs changed when

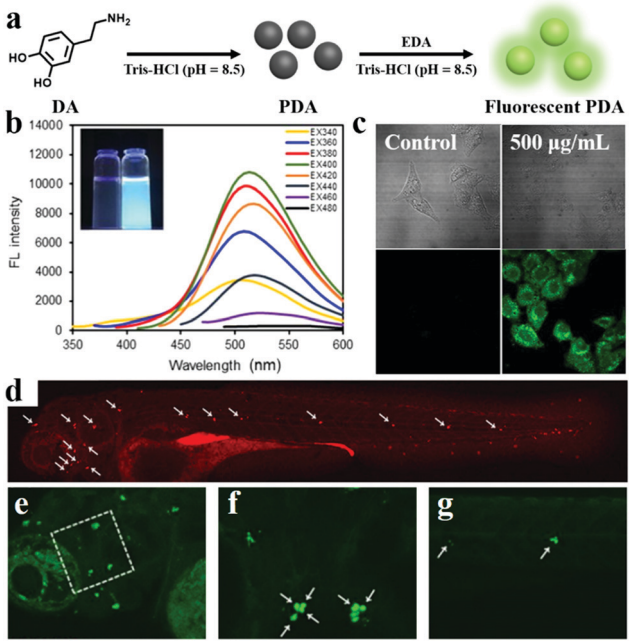

Fig. 13 (a) Schematic illustration of the fluorescent PDA synthesis. (b) Fluorescence emission spectra under different excitation wavelengths. (c) Confocal fluorescence images of living HeLa cells incubated with the fluorescent PDA. (d) Fluorescence image of sensory hair cells in the lateral line of whole zebrafish larvae. The panels (e–g) show the cells stained with fluorescent PDA. The enlarged image of the white boxed areas in (e) correspond to (f). Scale bars: 200 μm (d), 50 μm (e and f), and 100 μm (g).[69] Copyright 2018 Springer Nature.

excitation wavelength varied from 340 nm to 480 nm and reached its maximum when excited at 400 nm. Furthermore, the fluorescence intensity of the PDA NP solution did not change after continuous irradiation at 490 nm by a steady-state xenon lamp for 3000 s, indicating the excellent photostability for *in vivo* fluorescence detection. These advantages of the fluorescent PDA NPs offer the potential for real-time monitoring of functional cell transplantation and therapies based on cells.

In nanomedicine, chemo- and phototherapy have been developed to combine with real time bioimaging for theranostics. Fluorescent PDA materials are promising for use as theranostic agents due to their abundant surface chemistry. The surface of PDA materials is rich in functional groups (*e.g.* catechol, carboxyl, carbonyl and amino groups) and aromatic rings, endowing the abilities to chelate metal ions, absorb hydrophobic drugs, react with other groups, and initiate polymerizations.[110–113] Interestingly, the fluorescent PDA NPs showed different fluorescence under distinct buffer conditions for diagnostic purposes.[78] In neutral buffers, the emission wavelengths of fluorescent PDA NPs became wider with low intensity and became stronger under acidic conditions, allowing their use for monitoring tumor environments. By integration with the inherent photothermal conversion capability of PDA, fluorescent PDA materials have been applied to synergistically trigger pH-responsive photothermal and chemotherapeutic platforms in the extracellular tumor environment.[78]

In addition, fluorescent PDA can also be prepared by the incorporation of fluorescent dye molecules in PDA NPs. This has offered a versatile imaging and therapeutic platform with options from UV to the NIR region that is hard to achieve by structural engineering of PDA. For example, Liu's group developed a theranostic nano-platform based on PDA NPs *via* π–π stacking and hydrophobic interaction.[29] After incubation with 4T1 cells, a higher fluorescence signal was found in the treated cells under NIR light, which also was proved by flow cytometer data. However, the FRET effect induced by the quinone residues on the PDA surface could quench the fluorescence of the dye, hindering effective medical imaging and theranostics in the working concentration range. To eliminate the FRET effect and enhance the fluorescence, organic ligands and coatings such as PEG and SiO_2 have been employed to increase the distance between PDA and dye, as well as improve bioavailability of PDA.[114] Recently, Zhang *et al.* reported a PDA-based nanoplatform using a surface-initiated atom transfer radical polymerization (ATRP) strategy that showed excellent fluorescence imaging performance *via* conjugation with a fluorescent Eu(III) complex (Fig. 14).[97] First, confocal laser scanning microscopy was used to monitor the cellular internalization of the fluorescent PDA in 4T1 cells. The results showed the accumulation of PDA in the cytoplasm. The fluorescence intensity increased with incubation time, suggesting continuous internalization of PDA. Furthermore, the time-dependent fluorescence intensity distribution was evaluated after intravenous injection. Livers showed an obvious increase in fluorescence intensity at 8 h after intravenous injection, while the fluorescence intensity gradually decreased from 12 h

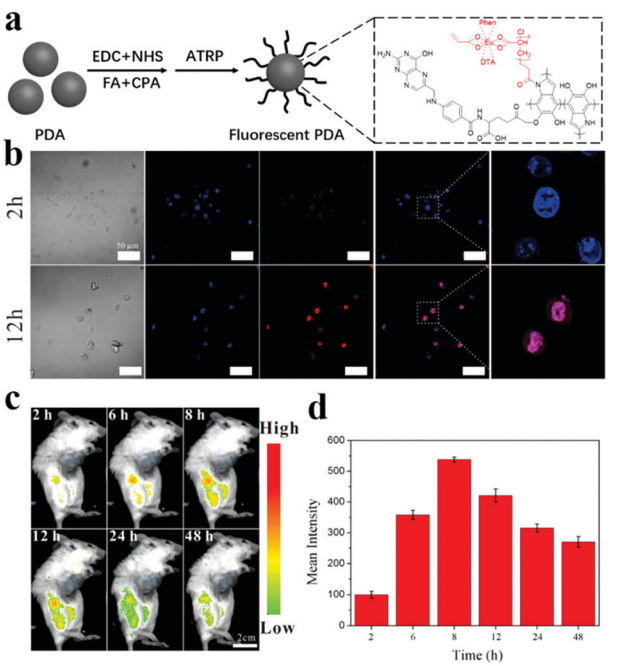

Fig. 14 (a) Schematic illustration of the fluorescent PDA synthesis. (b) Cellular internalization analysis. (c) *In vivo* fluorescence imaging. (d) Fluorescence signal intensities at kidney region.[97] Reprinted with permission from ref. 97. Copyright 2019 American Chemical Society.

after injection. Compared with conventional clinical agents, fluorescent PDA showed prominent imaging properties and outstanding biocompatibility, making it promising for potential bioscience applications.

4.2 High-resolution display

Display techniques usually employ electronic technology to provide flexible visual information, meeting practical demands *via* changing of intensity, wavelength, and other characteristics of light. However, the undulatory property of light still limits the resolution. High-resolution imaging techniques are maturing and provide opportunities for better observation in more detail.[115] Our group has demonstrated the application of fluorescent PDA materials as electronic ink for high-resolution display techniques, showing low power consumption (operation voltage of only 1 V) in aqueous solutions (Fig. 15).[53] The fluorescent PDA NPs were synthesized through the simple oxidation (H_2O_2) of PDA NPs for 24 h. The fluorescent micropatterns displayed were characterized under a fluorescence microscope, showing clear images with nanoscale resolution (10 000 ppi), since single particles were directly used in electrophoretic displays.[116,117] In combination with a fluorescence display, the electronic ink display devices could provide a unique dual-channel for visualization. The high dispersion and aqueous stability of the fluorescent PDA materials are the two key points to realize a nanoscale fluorescence display with this system.[53] In another example, PDA was used to functionalize a fluorescent nanodiamond surface for long-term, high-resolution single-molecule fluorescence-based tracking measurements.[118] After PDA encapsulation, the enhanced dispersion and stability of the samples benefited the internalization in cells. However, PDA might quench the fluorescence of nanodiamonds *via* FRET mechanism. Optimizing the reaction conditions to achieve a minimum shell thickness of PDA helped retain the maximum fluorescence intensity by reducing photoluminescence losses from the quenching and absorption of PDA. The PDA-based fluorescent materials not only perform with remarkable optical properties but offer specific binding groups for further functionalization.

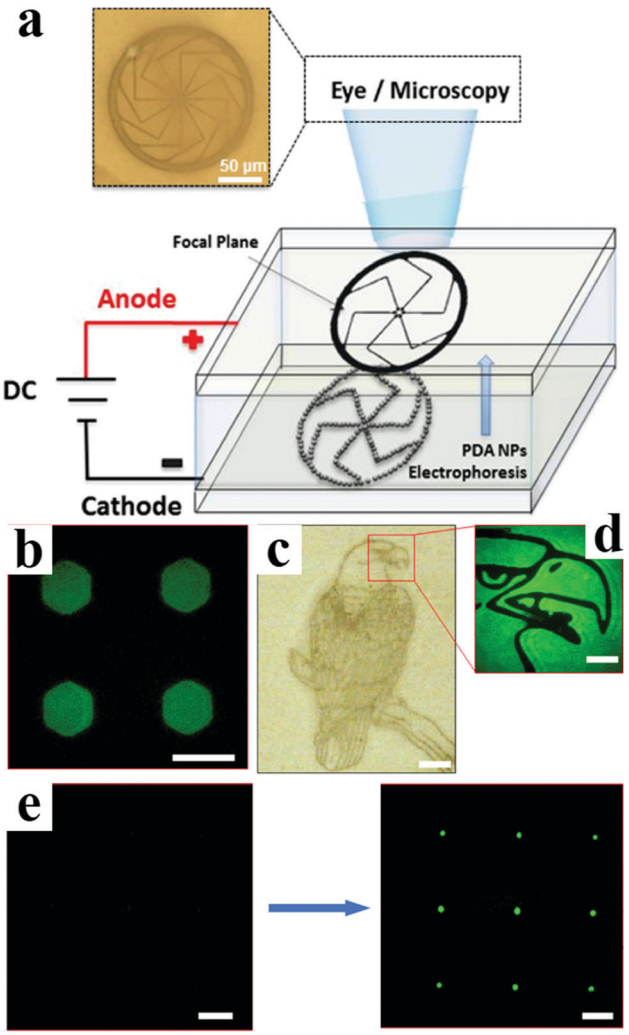

Fig. 15 (a) Schematic illustration of the PDA E-ink-based device for display. (b) Fluorescence display of hexagonal micropatterns. (c and d) Fluorescent PDA NP-supported displays with dual channels for an image. (e) A nanocircle array, 500 nm in diameter, was patterned on top of ITO film. Scale bars: (b) 10 μm, (c) 100 μm, (d) 30 μm, and (e) 10 μm.[53] Reprinted with permission from ref. 53. Copyright 2017 American Chemical Society.

4.3 Sensing for biomolecules

Biomolecules play important roles in biochemical processes. To date, various nanomaterials have been developed for biomolecule sensing, including gold NPs, carbon nanomaterials (*e.g.*, carbon NPs, carbon nanotubes, and graphene oxide), and metal–organic frameworks (MOF).[119–121] However, gold NPs require many surface functionalization processes since it is difficult to simultaneously adsorb biomolecules. The fabrication processes of carbon nanomaterials and MOF also have many disadvantages, such as being time-consuming and labor-intensive. More importantly, the long-term stability and toxicity of these materials are still concerns for clinical use. As alternatives, fluorescent PDA offered rapid, direct and cost-effective approaches for detection of biomolecules including DA, proteins, adenosine triphosphate (ATP) and alkaline phosphatase (ALP) *via* monitoring fluorescence intensity changes.[51,65,122–125] For instance, Yildirim *et al.* developed a facile assay for detection of DA based on the fluorescence intensity increase after DA polymerization (Fig. 16).[50] However, the high activity of DA might result in the generation of aggregates and quench the fluorescence. Thus, excess acid was added to stop the reaction and obtain stable fluorescence. After acid addition, the fluorescence intensity increased slightly and remained steady for at least 45 min. Furthermore, the fluorescence intensity at 510 nm was found to have a linear correlation with DA concentration, which was used in the assay for DA detection. The assay also showed high selectivity even at high concentrations of interfering chemicals (10-fold). Compared with other DA detection methods, this method is extremely facile and low cost, making it promising for practical application in complex environments.

A similar strategy was utilized in another work by Zheng's group, in which ficin was employed as a peroxidase-mimic to

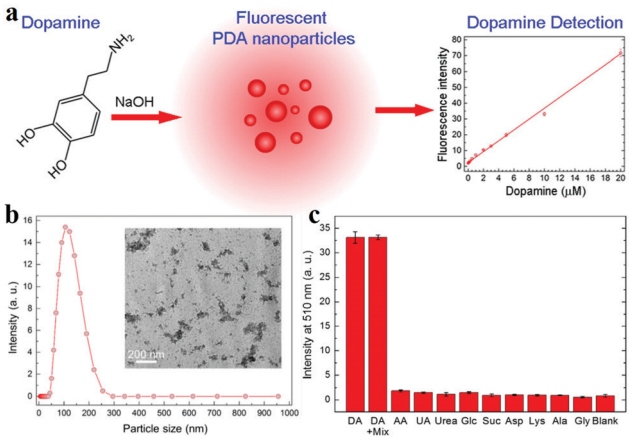

Fig. 16 (a) Schematic illustration of fluorescent PDA formation for DA detection. (b) Size distribution of fluorescent PDA NPs. Inset shows the TEM image of the NPs. (c) Selectivity of the dopamine assay.[50] Reprinted with permission from ref. 50. Copyright 2014 American Chemical Society.

synthesize fluorescent PDA NPs.[58] It is worth noting that the concentration of H_2O_2 used was as low as 40 μM. They found that no fluorescence signal existed in the presence of free DA, DA with ficin or DA with H_2O_2. However, a distinct fluorescence signal was observed when DA was mixed with H_2O_2 and ficin together, because ficin could efficiently convert H_2O_2 into a hydroxyl radical, which was then consumed by the oxidation process of DA. Furthermore, Yu *et al.* utilized another approach to detect DA by synthesizing red-emission CdTe@SiO_2 as the core and green-emission PDA as the shell.[71] Both CdTe@SiO_2 and PDA had strong fluorescence with emission peaks centered at 654 nm and 508 nm, respectively. After the addition of DA, the intensity at 508 nm gradually increased while the fluorescence intensity at 654 nm did not change. We reasoned that the additional DA could convert into a fluorescent part with the NPs, leading to enhancement of the green fluorescence intensity, but did not influence the red fluorescence from the core. At the same time, the color of the solution also changed from green to red. Compared with the fluorescence spectroscopy method, the dual-emission fluorescence probe had distinct superiority for visual sensing of DA.

Other biological small molecules were also detected by PDA-based fluorescent materials.[60] For instance, the detection of GSH, the most abundant nonprotein molecule in the cell, has become an important subject. Kong and co-workers established a cost-effective sensor for rapid, sensitive and selective sensing of reduced GSH using fluorescent PDA-based NPs as a fluorescence signal indicator.[59] The presence of GSH could inhibit the oxidation of DA induced by an oxidant, resulting in a loss of fluorescence. The sensor exhibited high sensitivity and desirable selectivity over other potential interfering species for GSH detection. The fluorescence intensity at 485 nm decreased gradually with increasing GSH concentration in the range from 0 to 800 μM. Importantly, a linear response was obtained in the range from 0 to 350 μM with a detection limit of 1.5 μM.[59] Moreover, the as-prepared sensor exhibited an increase of fluorescence intensity in the presence of GSH while showing no or only slight fluorescence intensity increase with other potential interference compounds, such as metal ions or amino acids, making it promising for further applications in human whole blood samples.

4.4 Sensing for metal ions

PDA consists of abundant catechol functional groups that display strong affinity for metal ions such as Fe^{3+}, Mg^{2+}, Ca^{2+}, Zn^{2+}, Cu^{2+}, *etc.*[126] After coordination, the fluorescence of PDA materials changes due to the change of electron configuration in PDA. Therefore, fluorescent PDA materials can be used to detect the metal ions that induced its fluorescence change. This phenomenon has been used in heavy metal detection in water, including for Cu^{2+}, Zn^{2+}, Al^{3+}, Fe^{3+}, Cr^{6+}, and U^{6+}.[66] Zhao *et al.* reported the reversible redox process of the fluorescent PDA in the presence of Cr^{6+} which can be used as for detection.[64] Subsequently, they studied the ability of the probe to sense different oxidizing agents ($K_2Cr_2O_7$, $NaCrO_4$, $KMnO_4$, H_2O_2, HNO_3, NaClO, and Cl_2). However, only $K_2Cr_2O_7$ and $NaCrO_4$ can effectively quench the fluorescence, which might be attributed to differences in the reduction potential of Cr^{6+}. Moreover, Lin and co-workers reported the fluorescence quenching phenomenon of fluorescent PDA after coordination with Fe^{3+}.[49] They believe that the mechanism of the fluorescence quenching involved electron transfer from the excited state of PDA NPs to an unfilled d shell of Fe^{3+}. In that work, the detection limit was determined to be as low as 0.3 μM,[49] suitable for application as an optical sensor to sense Fe^{3+} in the public health field. Ravikumar *et al.* prepared fluorescent PDA under mild conditions with the aid of exonuclease III to assist in signal amplification for ultra-selective recognition (detection limit 10 pM) of Hg^{2+}.[127] In contrast, metal ions can also enhance the fluorescence property of PDA. It was reported that Zn^{2+} can enhance the fluorescence of obtained particles under 360 nm excitation but not under 480 nm excitation, which might be related to photo-induced electron or charge transfer, making the particles promising for sensing Zn^{2+}.[56] The Zn^{2+} probe was first synthesized by DA oxidation catalyzed by Fe_3O_4 (Fig. 17). Different from traditional strategies using multiple steps with ~6% H_2O_2, the Fe_3O_4 catalyzed oxidation over a wide temperature range and required only 5 mM H_2O_2, about 400 times less than the previous literature. Interestingly, only the fluorescent PDA incubated with Zn^{2+} exhibited strong blue emission under UV lamp. The fluorescent PDA incubated with Zn^{2+} also possessed a strong emission intensity in the fluorescence spectra. The fluorescence intensity showed a linear function for Zn^{2+} concentration in a wide range from 60 nM to 5 μM in a complex mixture, suggesting that the sensor could be proposed for Zn^{2+} detection in complex environments.

The reversible nature of metal ion and catechol coordination enabled the fabrication of fluorescence-based logic gates. Luo and co-workers built a logic gate with Fe^{3+} and pyrophosphate (PPi) as inputs and the fluorescence signal of the PDA NPs as output.[74] After Fe^{3+} chelation with PDA, the electron derived from the excited state of PDA easily transfers to the unoccupied d-orbitals of Fe^{3+}, thus quenching the fluorescence

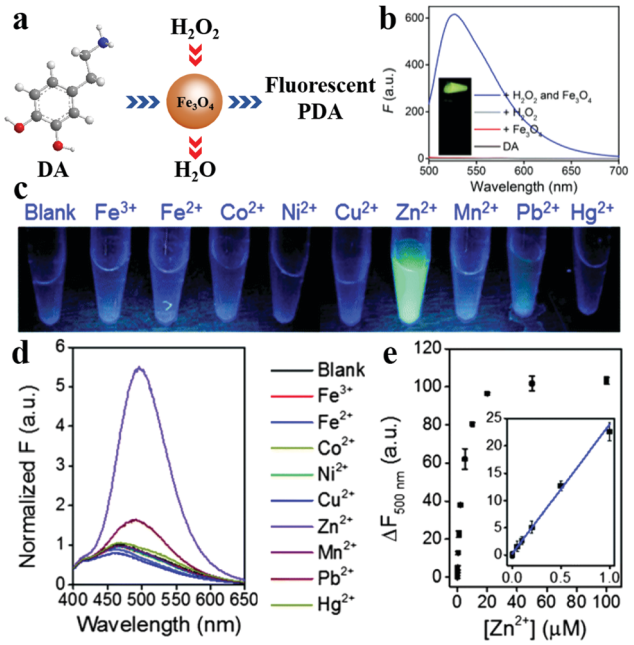

Fig. 17 (a) Schematic illustration of the preparation of fluorescent PDA using Fe_3O_4 NPs as a peroxidase mimicking nanozyme. (b) Fluorescence emission spectra (excitation at 480 nm) of fluorescent PDA and control samples. The inset photograph shows the samples under 470 nm excitation. (c) Fluorescence images of fluorescent PDA in the presence of various metal ions (10 μM) under 360 nm excitation. (d) The corresponding fluorescence spectra under 360 nm excitation. (e) Fluorescence intensity as a function of Zn^{2+} concentration.[56] Reproduced from ref. 56 with permission from the Royal Society of Chemistry.

of the PDA. In contrast, the addition of PPi induced fluorescence recovery due to the formation of $Fe_4(P_2O_7)_3$. Therefore, the relative concentrations of Fe^{3+} and PPi can be evaluated. This system showed good repeatability, maintaining 10 regeneration cycles of alternately adding Fe^{3+} and PPi.

In addition, fluorescent PDA materials could be applied to the combination of biochemical detection and biological imaging. Wu's group employed fluorescent dopamine-derived oligomers for selective detection of Fe^{3+} and targeted bioimaging.[48] The detection limit of Fe^{3+} is 0.1 μM, much lower than the maximum level permitted in drinking water by the US Environmental Protection Agency.

5. Summary and outlook

This feature article attempted to summarize the latest research progress in fluorescent PDA materials, from fabrication strategies, morphologies, and surface modifications to their promising applications in bioimaging and sensing. Since 2012, developing fluorescent PDA materials has been popular in biomedical applications. However, there are still problems that need to be overcome in the future for application in clinical practice, although impressive advances have been made. First, the exact mechanism of fluorescence generation in PDA is still unclear due to the lack of precise detailed microstructural information, which also hinders the preparation of novel fluorescent PDA materials with superior properties. We believe that new techniques can be applied to characterize and identify the microscopic structural information within PDA in the near future. Second, the morphologies of fluorescent PDA materials are not well-controlled, which could cause the brightness and diffusion coefficients to be heterogeneous, limiting quantitative imaging for bio-applications. Another potential problem is the scattering interference of particles, which has not been well addressed. Third, the immunogenicity and long-term toxicity of fluorescent PDA materials should be completely evaluated to pave the way for their promising future in the fields of biology and medicine. The related *in vivo* research has not been completely carried out. Lastly, the increasingly stringent requirements imposed by regulatory bodies in biological and environmental analysis have been urging higher selectivity and sensitivity, which could make fluorescent PDA materials fall short in specific practical applications. So, these challenges need versatile fluorescent PDA materials, induced by different sources, such as NIR, with superior properties.

We hope that this feature article has offered a comprehensive overview of the synthesis, fluorescence properties and applications of fluorescent PDA, providing guidance to the researchers working in this field to design the next-generation fluorescent PDA nanomaterials and their related applications.

Conflicts of interest

There are no conflicts to declare.

Acknowledgements

This work was supported by National Natural Science Foundation of China (21774079 and 21975167), State Key Laboratory Cultivation Base for Nonmetal Composites and Functional Materials, Southwest University of Science and Technology (17kffk07), State Key Laboratory of Polymer Materials Engineering, Sichuan University (sklpme2018-2-04), and the Fundamental Research Funds for Central Universities.

Notes and references

1 Y. Liu, K. Ai and L. Lu, *Chem. Rev.*, 2014, **114**, 5057–5115.
2 M. Liu, G. Zeng, K. Wang, Q. Wan, L. Tao, X. Zhang and Y. Wei, *Nanoscale*, 2016, **8**, 16819–16840.
3 Y. Zou, Z. Wang, Z. Chen, Q.-P. Zhang, Q. Zhang, Y. Tian, S. Ren and Y. Li, *J. Phys. Chem. C*, 2019, **123**, 5345–5352.
4 P. Yang, S. Zhang, N. Zhang, Y. Wang, J. Zhong, X. Sun, Y. Qi, X. Chen, Z. Li and Y. Li, *ACS Appl. Mater. Interfaces*, 2019, **11**, 42671–42679.
5 H. Lee, S. M. Dellatore, W. M. Miller and P. B. Messersmith, *Science*, 2007, **318**, 426–430.
6 L. Yang, B. Gu, Z. Chen, Y. Yue, W. Wang, H. Zhang, X. Liu, S. Ren, W. Yang and Y. Li, *ACS Appl. Mater. Interfaces*, 2019, **11**, 30360–30367.

7 T. G. Barclay, H. M. Hegab, S. R. Clarke and M. Ginic-Markovic, *Adv. Mater. Interfaces*, 2017, **4**, 1601192.
8 S. M. Kang, I. You, W. K. Cho, H. K. Shon, T. G. Lee, I. S. Choi, J. M. Karp and H. Lee, *Angew. Chem., Int. Ed.*, 2010, **49**, 9401–9404.
9 N. Patil, C. Jérôme and C. Detrembleur, *Prog. Polym. Sci.*, 2018, **82**, 34–91.
10 D. R. Dreyer, D. J. Miller, B. D. Freeman, D. R. Paul and C. W. Bielawski, *Chem. Sci.*, 2013, **4**, 3796–3802.
11 X. Wang, Z. Chen, P. Yang, J. Hu, Z. Wang and Y. Li, *Polym. Chem.*, 2019, **10**, 4194–4200.
12 J. Jiang, L. Zhu, L. Zhu, B. Zhu and Y. Xu, *Langmuir*, 2011, **27**, 14180–14187.
13 J. H. Ryu, P. B. Messersmith and H. Lee, *ACS Appl. Mater. Interfaces*, 2018, **10**, 7523–7540.
14 Q. Ye, F. Zhou and W. Liu, *Chem. Soc. Rev.*, 2011, **40**, 4244–4258.
15 K. Qu, Y. Wang, A. Vasileff, Y. Jiao, H. Chen and Y. Zheng, *J. Mater. Chem. A*, 2018, **6**, 21827–21846.
16 X. Wang, J. Zhang, Y. Wang, C. Wang, J. Xiao, Q. Zhang and Y. Cheng, *Biomaterials*, 2016, **81**, 114–124.
17 Z. Zhou, Y. Yan, L. Wang, Q. Zhang and Y. Cheng, *Biomaterials*, 2019, **203**, 63–72.
18 S. Wang, J. Lin, Z. Wang, Z. Zhou, R. Bai, N. Lu, Y. Liu, X. Fu, O. Jacobson, W. Fan, J. Qu, S. Chen, T. Wang, P. Huang and X. Chen, *Adv. Mater.*, 2017, **29**, 1701013.
19 K. Ai, Y. Liu, C. Ruan, L. Lu and G. M. Lu, *Adv. Mater.*, 2013, **25**, 998–1003.
20 C. Qi, L.-H. Fu, H. Xu, T.-F. Wang, J. Lin and P. Huang, *Sci. China: Chem.*, 2019, **62**, 162–188.
21 Y. Wang, Q. Huang, X. He, H. Chen, Y. Zou, Y. Li, K. Lin, X. Cai, J. Xiao, Q. Zhang and Y. Cheng, *Biomaterials*, 2018, **183**, 10–19.
22 Z. Zhou, Y. Yan, K. Hu, Y. Zou, Y. Li, R. Ma, Q. Zhang and Y. Cheng, *Biomaterials*, 2017, **141**, 116–124.
23 Z. Wang, F. Carniato, Y. Xie, Y. Huang, Y. Li, S. He, N. Zang, J. D. Rinehart, M. Botta and N. C. Gianneschi, *Small*, 2017, **13**, 1701830.
24 A. Liopo, R. Su and A. A. Oraevsky, *Photoacoustics*, 2015, **3**, 35–43.
25 D. L. Longo, R. Stefania, S. Aime and A. Oraevsky, *Int. J. Mol. Sci.*, 2017, **18**, 1719.
26 H. Zhuang, H. Su, X. Bi, Y. Bai, L. Chen, D. Ge, W. Shi and Y. Sun, *ACS Biomater. Sci. Eng.*, 2017, **3**, 1799–1808.
27 P. Zhang, Y. Yue, D. Pan, R. Yang, Y. Xu, L. Wang, J. Yan, X. Li and M. Yang, *Nucl. Med. Biol.*, 2016, **43**, 529–533.
28 P. Meredith and J. Riesz, *Photochem. Photobiol.*, 2004, **79**, 211–216.
29 Z. Dong, H. Gong, M. Gao, W. Zhu, X. Sun, L. Feng, T. Fu, Y. Li and Z. Liu, *Theranostics*, 2016, **6**, 1031–1042.
30 C. Wang, D. Wang, T. Dai, P. Xu, P. Wu, Y. Zou, P. Yang, J. Hu, Y. Li and Y. Cheng, *Adv. Funct. Mater.*, 2018, **28**, 1802127.
31 S. Ma, Y. X. Qi, X. Q. Jiang, J. Q. Chen, Q. Y. Zhou, G. Shi and M. Zhang, *Anal. Chem.*, 2016, **88**, 11647–11653.
32 D. Fan, C. Wu, K. Wang, X. Gu, Y. Liu and E. Wang, *Chem. Commun.*, 2016, **52**, 406–409.
33 W. Qiang, W. Li, X. Li, X. Chen and D. Xu, *Chem. Sci.*, 2014, **5**, 3018–3024.
34 X. Ji, G. Palui, T. Avellini, H. B. Na, C. Yi, K. L. Knappenberger, Jr. and H. Mattoussi, *J. Am. Chem. Soc.*, 2012, **134**, 6006–6017.
35 I. L. Medintz, M. H. Stewart, S. A. Trammell, K. Susumu, J. B. Delehanty, B. C. Mei, J. S. Melinger, J. B. Blanco-Canosa, P. E. Dawson and H. Mattoussi, *Nat. Mater.*, 2010, **9**, 676–684.
36 X. Zhang, S. Wang, L. Xu, L. Feng, Y. Ji, L. Tao, S. Li and Y. Wei, *Nanoscale*, 2012, **4**, 5581–5584.
37 A. Qin, J. W. Y. Lam and B. Z. Tang, *Prog. Polym. Sci.*, 2012, **37**, 182–209.
38 L.-C. Mao, X.-Y. Zhang and Y. Wei, *Chin. J. Polym. Sci.*, 2019, **37**, 340–351.
39 S. Hong, Y. S. Na, S. Choi, I. T. Song, W. Y. Kim and H. Lee, *Adv. Funct. Mater.*, 2012, **22**, 4711–4717.
40 E. A. Jares-Erijman and T. M. Jovin, *Nat. Biotechnol.*, 2003, **21**, 1387–1395.
41 Y. Hong, J. W. Y. Lam and B. Z. Tang, *Chem. Soc. Rev.*, 2011, **40**, 5361–5388.
42 G. Perna, M. C. Frassanito, G. Palazzo, A. Gallone, A. Mallardi, P. F. Biagi and V. Capozzi, *J. Lumin.*, 2009, **129**, 44–49.
43 M. d'Ischia, A. Napolitano, V. Ball, C. T. Chen and M. J. Buehler, *Acc. Chem. Res.*, 2014, **47**, 3541–3550.
44 P. Meredith and T. Sarna, *Pigm. Cell Res.*, 2006, **19**, 572–594.
45 P. Meredith, B. J. Powell, J. Riesz, S. P. Nighswander-Rempel, M. R. Pederson and E. G. Moore, *Soft Matter*, 2006, **2**, 37–44.
46 Z. Xu, N. J. Singh, J. Lim, J. Pan, H. N. Kim, S. Park, K. S. Kim and J. Yoon, *J. Am. Chem. Soc.*, 2009, **131**, 15528–15533.
47 C. Pan, K. Sugiyasu, Y. Wakayama, A. Sato and M. Takeuchi, *Angew. Chem., Int. Ed.*, 2013, **52**, 10775–10779.
48 B. Xiong, Y. Chen, Y. Shu, B. Shen, H. N. Chan, Y. Chen, J. Zhou and H. Wu, *Chem. Commun.*, 2014, **50**, 13578–13580.
49 J. H. Lin, C. J. Yu, Y. C. Yang and W. L. Tseng, *Phys. Chem. Chem. Phys.*, 2015, **17**, 15124–15130.
50 A. Yildirim and M. Bayindir, *Anal. Chem.*, 2014, **86**, 5508–5512.
51 T. Xiao, J. Sun, J. Zhao, S. Wang, G. Liu and X. Yang, *ACS Appl. Mater. Interfaces*, 2018, **10**, 6560–6569.
52 Q. Ci, J. Liu, X. Qin, L. Han, H. Li, H. Yu, K. L. Lim, C. W. Zhang, L. Li and W. Huang, *ACS Appl. Mater. Interfaces*, 2018, **10**, 35760–35769.
53 L. Chang, F. Chen, X. Zhang, T. Kuang, M. Li, J. Hu, J. Shi, L. J. Lee, H. Cheng and Y. Li, *ACS Appl. Mater. Interfaces*, 2017, **9**, 16553–16560.
54 X. Chen, Y. Yan, M. Mullner, M. P. van Koeverden, K. F. Noi, W. Zhu and F. Caruso, *Langmuir*, 2014, **30**, 2921–2925.
55 B. Ma, F. Liu, S. Zhang, J. Duan, Y. Kong, Z. Li, D. Tang, W. Wang, S. Ge, W. Tang and H. Liu, *J. Mater. Chem. B*, 2018, **6**, 6459–6467.

56 B. Liu, X. Han and J. Liu, *Nanoscale*, 2016, **8**, 13620–13626.
57 Z. Lin, M. Li, S. Lv, K. Zhang, M. Lu and D. Tang, *J. Mater. Chem. B*, 2017, **5**, 8506–8513.
58 Y. Pang, Y. Shi, Y. Pan, Y. Yang, Y. Long and H. Zheng, *Sens. Actuators, B*, 2018, **263**, 177–182.
59 X. J. Kong, S. Wu, T. T. Chen, R. Q. Yu and X. Chu, *Nanoscale*, 2016, **8**, 15604–15610.
60 Y.-Y. Zhao, L. Li, R.-Q. Yu, T.-T. Chen and X. Chu, *Anal. Methods*, 2017, **9**, 5518–5524.
61 H. Yin, K. Zhang, L. Wang, K. Zhou, J. Zeng, D. Gao, Z. Xia and Q. Fu, *Nanoscale*, 2018, **10**, 18064–18073.
62 P. Ding, H. Wang, B. Song, X. Ji, Y. Su and Y. He, *Anal. Chem.*, 2017, **89**, 7861–7868.
63 J. Feng, Y. Chen, Y. Han, J. Liu, C. Ren and X. Chen, *Anal. Chim. Acta*, 2016, **926**, 107–117.
64 S. Z. Zhao, X. Song, X. M. Bu, C. Zhu, G. Wang, F. Liao, S. W. Yang and M. Wang, *J. Appl. Polym. Sci.*, 2017, **134**, 44784.
65 Q. Xue, X. Cao, C. Zhang and Y. Xian, *Microchim. Acta*, 2018, **185**, 231.
66 Z. Wang, C. Xu, Y. Lu, G. Wei, G. Ye, T. Sun and J. Chen, *Chem. Eng. J.*, 2018, **344**, 480–486.
67 Y. Liu, M. Yang, J. Li, W. Zhang and X. Jiang, *Anal. Chem.*, 2019, **91**, 6754–6760.
68 S. Quignard, M. d'Ischia, Y. Chen and J. Fattaccioli, *ChemPlusChem*, 2014, **79**, 1254–1257.
69 G. E. Gu, C. S. Park, H. J. Cho, T. H. Ha, J. Bae, O. S. Kwon, J. S. Lee and C. S. Lee, *Sci. Rep.*, 2018, **8**, 4393.
70 M. Liu, J. Ji, X. Zhang, X. Zhang, B. Yang, F. Deng, Z. Li, K. Wang, Y. Yang and Y. Wei, *J. Mater. Chem. B*, 2015, **3**, 3476–3482.
71 M. Yu, Y. Lu and Z. Tan, *Talanta*, 2017, **168**, 16–22.
72 C. Zhao, F. Zuo, Z. Liao, Z. Qin, S. Du and Z. Zhao, *Macromol. Rapid Commun.*, 2015, **36**, 909–915.
73 M. Chen, Q. Wen, F. Gu, J. Gao, C. C. Zhang and Q. Wang, *Chem. Eng. J.*, 2018, **342**, 331–338.
74 L. Tang, S. Mo, S. G. Liu, L. L. Liao, N. B. Li and H. Q. Luo, *Sens. Actuators, B*, 2018, **255**, 754–762.
75 L. Tang, S. Mo, S. G. Liu, N. Li, Y. Ling, N. B. Li and H. Q. Luo, *Sens. Actuators, B*, 2018, **259**, 467–474.
76 Y. Shi, D. Xu, M. Liu, L. Fu, Q. Wan, L. Mao, Y. Dai, Y. Wen, X. Zhang and Y. Wei, *Mater. Sci. Eng., C*, 2018, **82**, 204–209.
77 S. H. Kim, S. M. Sharker, H. Lee, I. In, K. D. Lee and S. Y. Park, *RSC Adv.*, 2016, **6**, 61482–61491.
78 S. H. Kim, I. In and S. Y. Park, *Biomacromolecules*, 2017, **18**, 1825–1835.
79 Z. A. I. Mazrad, C. A. Choi, Y. M. Kwon, I. In, K. D. Lee and S. Y. Park, *ACS Appl. Mater. Interfaces*, 2017, **9**, 33317–33326.
80 T. An, N. Lee, H.-J. Cho, S. Kim, D.-S. Shin and S.-M. Lee, *RSC Adv.*, 2017, **7**, 30582–30587.
81 S. K. Das, Y. Liu, S. Yeom, D. Y. Kim and C. I. Richards, *Nano Lett.*, 2014, **14**, 620–625.
82 J. Huang, J. Chen, T. Yao, J. He, S. Jiang, Z. Sun, Q. Liu, W. Cheng, F. Hu, Y. Jiang, Z. Pan and S. Wei, *Angew. Chem., Int. Ed.*, 2015, **54**, 8722–8727.
83 S. Zhu, J. Zhang, S. Tang, C. Qiao, L. Wang, H. Wang, X. Liu, B. Li, Y. Li, W. Yu, X. Wang, H. Sun and B. Yang, *Adv. Funct. Mater.*, 2012, **22**, 4732–4740.
84 A. Corani, A. Huijser, A. Iadonisi, A. Pezzella, V. Sundstrom and M. d'Ischia, *J. Phys. Chem. B*, 2012, **116**, 13151–13158.
85 J. Oshima, T. Yoshihara and S. Tobita, *Chem. Phys. Lett.*, 2006, **423**, 306–311.
86 C. Y. Liu and C. J. Huang, *Langmuir*, 2016, **32**, 5019–5028.
87 T. S. Sileika, H. D. Kim, P. Maniak and P. B. Messersmith, *ACS Appl. Mater. Interfaces*, 2011, **3**, 4602–4610.
88 H. Kwon, K. Lee and H. J. Kim, *Chem. Commun.*, 2011, **47**, 1773–1775.
89 E. Dumitriu, C. Guimon, A. Cordoneanu, S. Casenave, T. Hulea, C. Chelaru, H. Martinez and V. Hulea, *Catal. Today*, 2001, **66**, 529–534.
90 J. Zhang and S.-H. Yu, *Mater. Today*, 2016, **19**, 382–393.
91 Y. P. Sun, B. Zhou, Y. Lin, W. Wang, K. A. Fernando, P. Pathak, M. J. Meziani, B. A. Harruff, X. Wang, H. Wang, P. G. Luo, H. Yang, M. E. Kose, B. Chen, L. M. Veca and S. Y. Xie, *J. Am. Chem. Soc.*, 2006, **128**, 7756–7757.
92 J. Zhou, C. Booker, R. Li, X. Zhou, T. K. Sham, X. Sun and Z. Ding, *J. Am. Chem. Soc.*, 2007, **129**, 744–745.
93 W. Xiao, Y. Li, C. Hu, Y. Huang, Q. He and H. Gao, *J. Colloid Interface Sci.*, 2017, **497**, 226–232.
94 G. Eda, Y. Y. Lin, C. Mattevi, H. Yamaguchi, H. A. Chen, I. S. Chen, C. W. Chen and M. Chhowalla, *Adv. Mater.*, 2010, **22**, 505–509.
95 V. Ozhukil Kollath, M. Derakhshandeh, F. D. Mayer, T. Mudigonda, M. N. Islam, M. Trifkovic and K. Karan, *RSC Adv.*, 2018, **8**, 31967–31971.
96 Z. Li, T. Wang, F. Zhu, Z. Wang and Y. Li, *Chin. Chem. Lett.*, 2019, DOI: 10.1016/j.cclet.2019.05.021.
97 M. Zhang, Y. Zou, Y. Zhong, G. Liao, C. Yu and Z. Xu, *ACS Appl. Bio Mater.*, 2019, **2**, 630–637.
98 Z. Gan, H. Xu and Y. Hao, *Nanoscale*, 2016, **8**, 7794–7807.
99 L. Zhang, J. Shi, Z. Jiang, Y. Jiang, S. Qiao, J. Li, R. Wang, R. Meng, Y. Zhu and Y. Zheng, *Green Chem.*, 2011, **13**, 300–306.
100 B. Yu, D. A. Wang, Q. Ye, F. Zhou and W. Liu, *Chem. Commun.*, 2009, 6789–6791.
101 J. Xue, W. Zheng, L. Wang and Z. Jin, *ACS Biomater. Sci. Eng.*, 2016, **2**, 489–493.
102 F. Nador, E. Guisasola, A. Baeza, M. A. Villaecija, M. Vallet-Regi and D. Ruiz-Molina, *Chem. – Eur. J.*, 2017, **23**, 2753–2758.
103 D. Shi, L. Zhang, J. Shen, X. Li, M. Chen and M. Akashi, *RSC Adv.*, 2015, **5**, 103414–103420.
104 L. Huang, M. Liu, H. Huang, Y. Wen, X. Zhang and Y. Wei, *Biomacromolecules*, 2018, **19**, 1858–1868.
105 R. Weissleder, M. Nahrendorf and M. J. Pittet, *Nat. Mater.*, 2014, **13**, 125–138.
106 O. S. Wolfbeis, *Chem. Soc. Rev.*, 2015, **44**, 4743–4768.
107 C. Wang, J. Zhou, P. Wang, W. He and H. Duan, *Bioconjugate Chem.*, 2016, **27**, 815–823.
108 L. Zhang, R. Zhang, M. Gao and X. Zhang, *Talanta*, 2016, **158**, 315–321.

109 L. Yang, Y. Ren, W. Pan, Z. Yu, L. Tong, N. Li and B. Tang, *Anal. Chem.*, 2016, **88**, 11886–11891.
110 Y. Li, Y. Xie, Z. Wang, N. Zang, F. Carniato, Y. Huang, C. M. Andolina, L. R. Parent, T. B. Ditri, E. D. Walter, M. Botta, J. D. Rinehart and N. C. Gianneschi, *ACS Nano*, 2016, **10**, 10186–10194.
111 X. Wang, C. Wang, X. Wang, Y. Wang, Q. Zhang and Y. Cheng, *Chem. Mater.*, 2017, **29**, 1370–1376.
112 K. Y. Ju, Y. Lee, S. Lee, S. B. Park and J. K. Lee, *Biomacromolecules*, 2011, **12**, 625–632.
113 Z. Zeng, M. Wen, G. Ye, X. Huo, F. Wu, Z. Wang, J. Yan, K. Matyjaszewski, Y. Lu and J. Chen, *Chem. Mater.*, 2017, **29**, 10212–10219.
114 S. Cho, W. Park and D. H. Kim, *ACS Appl. Mater. Interfaces*, 2017, **9**, 101–111.
115 F. Huang, G. Sirinakis, E. S. Allgeyer, L. K. Schroeder, W. C. Duim, E. B. Kromann, T. Phan, F. E. Rivera-Molina, J. R. Myers, I. Irnov, M. Lessard, Y. Zhang, M. A. Handel, C. Jacobs-Wagner, C. P. Lusk, J. E. Rothman, D. Toomre, M. J. Booth and J. Bewersdorf, *Cell*, 2016, **166**, 1028–1040.
116 D. Graham-Rowe, *Nat. Photonics*, 2007, **1**, 248–251.
117 S. Harris, *Nat. Photonics*, 2010, **4**, 748–749.
118 H.-S. Jung, K.-J. Cho, Y. Seol, Y. Takagi, A. Dittmore, P. A. Roche and K. C. Neuman, *Adv. Funct. Mater.*, 2018, **28**, 1801252.
119 D. J. Maxwell, J. R. Taylor and S. Nie, *J. Am. Chem. Soc.*, 2002, **124**, 9606–9612.
120 J. N. Tiwari, V. Vij, K. C. Kemp and K. S. Kim, *ACS Nano*, 2016, **10**, 46–80.
121 Q. Zhang, C. F. Wang and Y. K. Lv, *Analyst*, 2018, **143**, 4221–4229.
122 J. Ge, D.-M. Bai, X. Geng, Y.-L. Hu, Q.-Y. Cai, K. Xing, L. Zhang and Z.-H. Li, *Microchim. Acta*, 2018, **185**, 105.
123 M. Yang, H. Zhou, Y. Zhang, Z. Hu, N. Niu and C. Yu, *Microchim. Acta*, 2018, **185**, 132.
124 W. Qiang, H. Hu, L. Sun, H. Li and D. Xu, *Anal. Chem.*, 2015, **87**, 12190–12196.
125 W. Qiang, X. Wang, W. Li, X. Chen, H. Li and D. Xu, *Biosens. Bioelectron.*, 2015, **71**, 143–149.
126 Y. J. Kim, W. Wu, S. E. Chun, J. F. Whitacre and C. J. Bettinger, *Adv. Mater.*, 2014, **26**, 6572–6579.
127 A. Ravikumar and P. Panneerselvam, *Analyst*, 2018, **143**, 2623–2631.